Combining Time-of-Flight Methods and Velocity-Aligned Doppler Spectroscopy to Measure Wavelength-Dependent Product State Distributions in H_2Se Photolysis†

Xiaodong Zhang, Michael Johnson, K. Thomas Lorenz, Kenneth A. Cowen, and Brent Koplitz*

Department of Chemistry, Tulane University, New Orleans, Louisiana 70118

Received: May 8, 2000; In Final Form: August 4, 2000

Results are presented on the ultraviolet photolysis of H_2Se. An experimental approach is introduced that combines velocity-aligned Doppler spectroscopy (VADS) with time-of-flight (TOF) methods. Atomic hydrogen is detected, and by utilizing a tunable photolysis source, one is able to map out propensities for populating HSe vibrational states as a function of photolysis wavelength. Interest in observing such behavior in triatomic systems was suggested theoretically by Schinke and co-workers in the mid-1980s.

I. Introduction

The field of chemical dynamics continues to grow more sophisticated in its ability to measure detailed product state distributions resulting from photodissociation. The number of systems that can be interrogated, the ways in which these systems can be explored, and the degree of correlation that one can observe between product states has evolved amazingly in the past 3 decades.[1] These advances are due in no small part to technological triumphs such as the tunable dye laser, but they are also due to pioneering practitioners in the field who have enabled technology to be implemented in innovative ways.[2−25] In this paper, we demonstrate how one can combine time-of-flight (TOF) methods with velocity-aligned Doppler spectroscopy (VADS) to measure correlated product state distributions. In the current study, the photolysis target is a polyatomic molecule (H_2Se) and the interrogated product is atomic hydrogen, but the approach does not appear to be restricted to these two systems.

There are several reasons for selecting H_2Se as a target molecule. It is one of the simplest metal-containing gaseous species that can be handled easily, and its excited-state dynamics may prove tractable computationally. It has a significant absorption cross section throughout the mid-ultraviolet region (unlike the more often studied group VI members H_2O and H_2S), thus H_2Se can be investigated with tunable photolysis sources having reasonable intensity. Finally, it is a good candidate to observe individual reactive scattering resonances as outlined theoretically for triatomic systems by Schinke and co-workers in the mid-1980s.[26] For a direct photodissociation process, there is a probability of scattering into each energetically available vibrational and rotational state in the diatomic fragment. In cases where the quantum yield for fragmentation is unity (or at least constant), a summation of the photolysis wavelength dependences for each quantum state yields the electronic absorption spectrum. However, as originally discussed by Schinke and co-workers, the individual vibrational state wavelength dependences may well contain interesting information on the dynamics of the dissociation process.[26] While subsequent work may have revised their initial theoretical treatment,[27] the underlying idea of investigating the wavelength dependence of scattering into individual vibrational states remains intriguing. In this paper, we show that the wavelength dependence of individual HSe vibrational channels resulting from H_2Se photolysis can indeed be measured, and the hybrid experimental method used to make these measurements is introduced.

Two decades ago, Welge and co-workers originally presented the use of 121.6 + 365 nm resonance ionization through Lyman-α as a means of detecting atomic hydrogen.[28] As a way of gaining insight into photodissociation events, the technique was coupled with a TOF approach to measure kinetic energy distributions (and by inference internal energy distributions) during the mid-1980s.[29] In this same time period, Wittig and co-workers developed the method known as velocity-aligned Doppler spectroscopy (VADS) and applied it to atomic hydrogen.[13] While the VADS method was being applied to systems other than atomic hydrogen,[30,31] a huge improvement in H atom detection was introduced again by Welge and co-workers in the late 1980s.[2] The Rydberg TOF method allowed one to avoid space-charge problems in the probe laser region, and the result was remarkable kinetic energy resolution. Throughout the 1990s, a number of groups have utilized this method to study systems where the H atom is the product of a photolysis event[32−34] as well as a bimolecular reactive event.[35]

As originally pioneered, the VADS method added a twist to conventional Doppler spectroscopy.[13] Instead of conducting a photolysis/probe experiment with a short delay and measuring a traditional, photofragment Doppler profile complete with all velocity projections on the probe axis, one simply delayed the two lasers sufficiently so that only those photofragments travelling forward or backward along the probe axis were sampled. This velocity alignment resulted in a dramatic change in the Doppler profile, since one could now observe discrete Doppler shifts correlated with the quantized energy deposition in the counterfragment. In the mid-1990s, Lorenz et al. enhanced the resolving power of the VADS method significantly by separating the photolysis and probe laser beams spatially.[36,37] By sacrificing one-half of the Doppler profile, which contains redundant information, and utilizing a ring laser as a probe, resolution improved by an order of magnitude. Moreover, one could now interrogate the nuclear hyperfine states of the species being probed, the H atom, and correlate these state distributions with the state distributions of the counterfragment, in this case the electronic states of Br. In the current paper, recent work on H_2Se photolysis is presented. In addition to straightforward TOF

† Part of the special issue "C. Bradley Moore Festschrift".

10.1021/jp001675r CCC: $19.00
Published on Web 09/20/2000

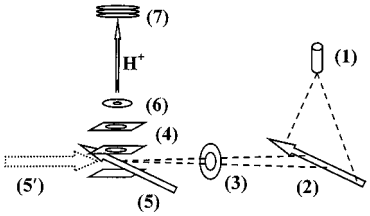

Figure 1. Schematic diagram of the experimental apparatus. The labels indicate (1) nozzle, (2) photolysis laser beam, (3) variable aperture, (4) ion extraction plates, (5) probe laser beam in TOF mode (H-configuration), (5′) probe laser beam in VADS mode (T-configuration), (6) ion aperture, (7) microchannel plate detector.

measurements, a further modification of the VADS method is introduced. Doppler spectra are taken in which the probe frequency and the probe delay are scanned synchronously. Also, the relationships between beam configuration, apertures, and resolution are briefly discussed.

II. Experimental Section

The basic experimental configuration is shown schematically in Figure 1. It is similar to that described previously,[36,37] but the current arrangement takes advantage of several important modifications. The photolysis of H_2Se in a supersonic expansion is initiated with the focused output of either the fourth harmonic (266 nm) of a Nd:YAG laser (Coherent Infinity; <0.1 cm^{-1} bandwidth at 266 nm) or the frequency-doubled output of a 355-nm-pumped broadband optical parametric oscillator (OPO) pumped by the third harmonic (355 nm) of the Nd:YAG laser. Commercially, this OPO is termed an XPO by its manufacturer, Coherent. Although it is relatively broad in frequency, the XPO is rather simple to use. In our experiments, the fundamental XPO output is typically $\sim$20$-$30 mJ/pulse over a range of 420 to 500 nm. We estimate that the ouput has a frequency bandwidth of $\sim$10$-$20 cm^{-1} over the doubled tuning range from 210 to 250 nm with a pulse energy of $\sim$1$-$2 mJ. The focusing lens used has a nominal focal length of 30 cm. In contrast to our previous work,[36,37] the flight distance to the probe region has been increased by an order of magnitude. A variable aperture (labeled (3) in Figure 1) adds an additional constraint to the velocity vectors that intersect the probe region. The species being detected, in this case the H atom, is probed in a second chamber at a distance 0.45 m from the point of photolysis. Here, the H atoms are ionized with probe laser radiation via 1+1′ (121.6 + 365 nm) resonance through Lyman-α. The probe pulse is generated in the following manner. The output of an Ar^+-pumped ring laser (Coherent 899$-$29; Ti:sapphire; 730 nm) is pulse amplified in three sequential excimer-pumped dye cuvettes. After frequency doubling in a BBO crystal, the resulting 365 nm radiation is pulse amplified and frequency tripled in Kr. Typical 365 nm pulse energies are $\sim$12$-$15 mJ, and the final 121.6 nm probe frequency bandwidth is estimated at <0.01 cm^{-1}.

In this modified experimental approach, the photolysis ($\mathbf{k_{ph}}$) and probe ($\mathbf{k_{pr}}$) directions of propagation can be arranged in either a parallel (H-configuration) or perpendicular (T-configuration) geometry, as shown in Figure 1 by the labels (5) and (5′), respectively. In the H-configuration, the approach becomes simply a high-resolution time-of-flight experiment. In this geometry, the probe laser is set at the zero-Doppler shift frequency of the H atom corresponding to the Lyman-α transition. Experimentally, one measures H^+ signal (and thus neutral H atom arrival) as a function of photolysis/probe delay time. Note that an aperture (labeled (6) in Figure 1) above the ionization region further defines the spatial region that is ultimately detected by the probe beam. In the T-configuration, a VADS experiment is conducted wherein both the probe laser frequency and photolysis/probe delay time must be adjusted so that H atoms with the desired Doppler shift are interrogated at the correct time in the ionization region. The VADS feature of the method permits one to scan the probe laser thereby positively identifying quantum states in the interrogated products. Here, the product states are the nuclear hyperfine states of the H atom.

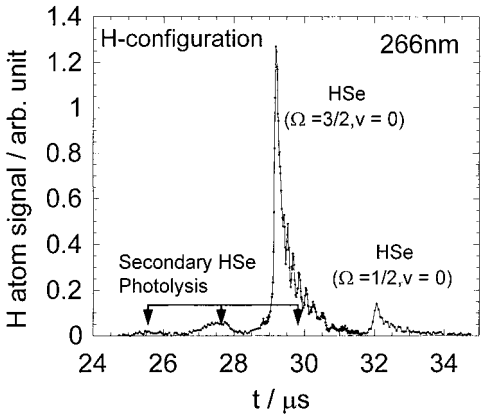

Figure 2. Survey TOF scan for H atom production after the 266 nm photolysis of H_2Se. The photolysis and probe laser beams were set in the H-configuration as shown in Figure 1, and the photolysis laser output was polarized vertically with respect to the axis traversed by the H atoms.

III. Results

When H_2Se molecules are photolyzed at a fixed frequency and produce H atoms, a variety of H atom speeds are produced due to the quantal nature of the HSe counterfragment. However, it must be emphasized that all references to HSe or Se state populations come about from inference. No HSe or Se detection was done in these experiments. In Figure 2, the results of a survey TOF scan for the 266 nm photolysis of H_2Se are shown. Here, $\mathbf{k_{ph}}$ and $\mathbf{k_{pr}}$ were set in the H-configuration, and H atom detection as a function of the delay between the photolysis and the probe lasers was monitored. The 266 nm laser output was vertically polarized with respect to the direction travelled by the nascent H atoms, and clear evidence for the formation of two spin$-$orbit HSe channels was observed. While rotational state populations are observable in each case, no significant vibrational population above $v = 0$ was identified for either state, although energetically 266 nm photolysis can populate up to $v = 4$ in the case of the HSe ground electronic state. As shown in Figure 2, secondary HSe photolysis channels resulting in H and Se in a variety of electronic states were also readily identified. Note too that changing the photolysis laser from vertical to horizontal polarization with respect to the product axis (not shown) dramatically changes the relative spin$-$orbit intensities in favor of the $\Omega = {}^1/_2$ state.

In Figure 3, a scan of the 29$-$31 μs delay region of Figure 2 is shown. Significant rotational population is observed in the $v = 0$ vibrational level of the $\Omega = {}^3/_2$ state, and the individual rotational state contributions used to simulate the spectrum can be seen in the underlying structure. Note, however, that the spectral features cannot be accurately simulated without inclusion of contributions from a secondary HSe photolysis channel as indicated. The rotational populations used to fit the data are included in Figure 4. For comparison purposes, rotational distributions for $v = 0$ of the $\Omega = {}^1/_2$ state are provided. Also

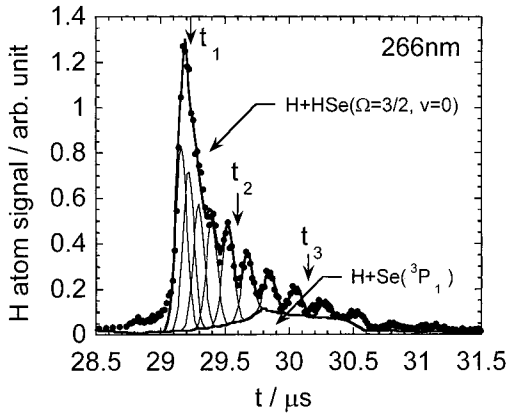

Figure 3. Expanded spectrum of the $\Omega = {}^3/_2$, $v = 0$ rotational manifold of Figure 2 showing experimental data along with individual simulation components. The primary heavy line constitutes the fit to the experimental data points. The rotational values used can be found in Figure 4, and the HSe photolysis contribution is as noted. Note also that the three selected delay times marked by arrows are associated with the three Doppler spectra shown in Figure 5.

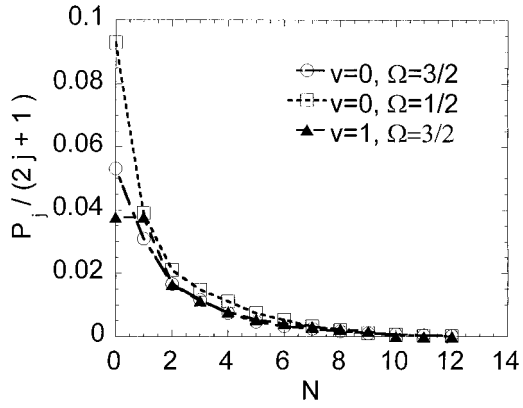

Figure 4. Rotational quantum state distributions extracted from experimental data for indicated HSe electronic and vibrational states. Each state examined had the same basic appearance for its rotational state distribution. Note: $\Sigma P_J = 1$ and $J = N + \Omega$.

shown is the rotational distribution for $v = 1$ of the $\Omega = {}^3/_2$ HSe manifold resulting from 225 nm photolysis. In all three cases, the rotational distributions are similar in appearance.

When only the rotational states of the HSe $\Omega = {}^3/_2$ channel were used to simulate the spectrum of Figure 3, it was not possible to achieve a good fit. The presence of an underlying contribution from a known HSe photolysis pathway was likely. To further examine this issue, studies were conducted with the photolysis and probe lasers in the T-configuration as described in Figure 1. Also, the T-configuration enabled us to examine the nuclear hyperfine states of the H atoms and correlate these populations with specific HSe product states. The results of three such studies are shown in Figure 5. For these studies, the arrows (t_1, t_2, and t_3) marked in Figure 3 indicate the corresponding delay time at which each Doppler scan was performed. Note that this particular experiment puts three constraints on an H atom that is being detected. After travelling ~450 mm, the H atom must be at a specific place at a specific time, and it must have the appropriate Doppler shift or it will not be detected. The laser beams as well as the apertures shown in Figure 1 place spatial constraints on the velocity vectors that can satisfy the time and frequency conditions.

For Figure 5, the $^2S_{1/2} \rightarrow {}^2P_{3/2}$ transition in Lyman-α was scanned. The inherent velocity alignment in the modified VADS method allows one to resolve the nuclear hyperfine (F states)

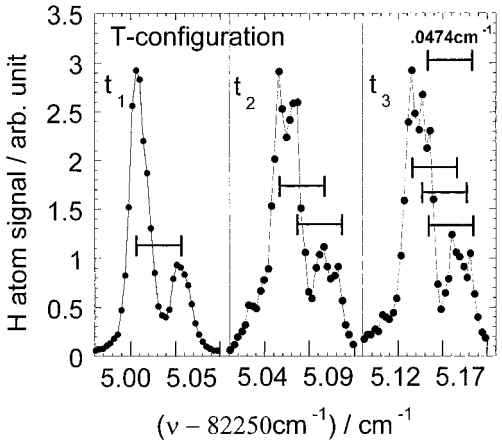

Figure 5. Doppler profiles for the $^2S_{1/2} \rightarrow {}^2P_{3/2}$ portion of the Lyman-α transition in atomic hydrogen. The T-configuration of Figure 1 was used, the flight distance was 450 mm, and the three different profiles correspond to the specific, fixed delay times marked in Figure 3. The greater spectral complexity for t_2 and t_3 can be attributed to H atoms correlated with separate HSe counterfragment states as well as HSe + $h\nu \rightarrow$ Se + H.

that are split by 0.0474 cm^{-1} in the ground state of atomic hydrogen.[38] For time t_1, which correlates with the HSe counterfragment being left behind in one of its low rotational states, the Doppler spectrum is basically smooth. Note, however, that the energy spacing between the lower HSe rotational levels is rather small, so in this region there are not discernible, discrete "packets" of H atoms arriving at the detection point. As is the case with 193 nm HBr photolysis,[36] within experimental error the nuclear hyperfine F states in the H atom appear to be populated equally, after accounting for degeneracy. In other words, there is no apparent dynamical bias toward populating one of the two states. At time t_2, which correlates with HSe counterfragments being left behind between their fifth and sixth rotational levels, the observed Doppler profile is composed of two overlapping, but slightly offset, sets of features. In each case, the features are split by 0.0474 cm^{-1}. Here, the "packets" of H atoms arriving at the detection point are distinguishable, since the energy spacing between rotational levels has increased. The correlation is apparent in the middle spectrum in Figure 5. One set of peaks corresponds to an HSe counterfragment in its fifth rotational state, while the other set can be attributed to HSe fragments in their sixth rotational state. However, once again, no dynamical bias is observed in the F-state populations.

For the region in the vicinity of time t_3 in Figure 3, the spectral fitting was particularly difficult when only H + HSe channels were used. This difficulty was surprising because the rotational energy spacing is large in this region. In fact, the Doppler profile for t_3 shown in Figure 5 helps explain the original fitting problem. This spectrum is not smooth at all, most likely because it contains several contributions including an H + Se ($^3P_1$) channel arising from the secondary photolysis of HSe. In effect, there are several H atom packets that arrive at slightly different times and have slightly different Doppler resonances. The resulting Doppler spectrum of Figure 5 is correspondingly not clear. Note that we do not think that the less than ideal spectrum arises from a signal-to-noise problem, although this possibility cannot be ruled out completely. Finally, if one adds a contribution from the known secondary photolysis channel in this region as shown in Figure 3, then the spectral fit for that data becomes much better.

Figures 6 and 7 present the results for H_2Se photolysis at four different wavelengths. Here, the frequency-doubled output

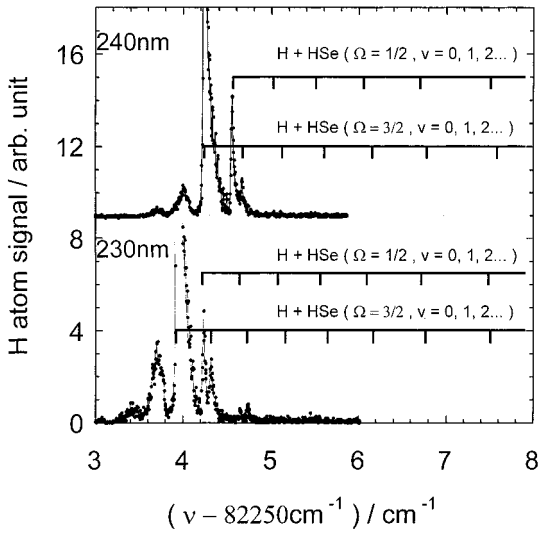

Figure 6. Doppler spectra taken at photolysis wavelengths of 240 and 230 nm with the photolysis/probe delay synchronously adjusted. The T-configuration of Figure 1 was used. Note that one can begin to see the emergence of HSe vibrational population for $v = 1$ and $v = 2$.

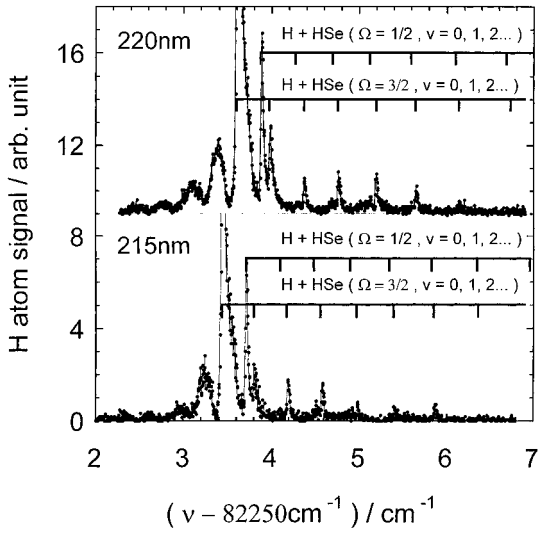

Figure 7. Doppler spectra taken at photolysis wavelengths of 220 and 210 nm with the photolysis/probe delay synchronously adjusted. The T-configuration of Figure 1 was used. When compared with Figure 6, note the significant increase in the population of the HSe vibrational quantum states as the photolysis wavelength is decreased.

of the Nd:YAG-pumped XPO was used. As in the case of Figure 5, the photolysis and probe lasers were set in the T-configuration. To acquire these spectra, the probe frequency was locked to a specific Lyman-α transition. To scan the spectrum, both the probe frequency and the photolysis/probe delay were scanned synchonously in order to satisfy the spatial, temporal, and Doppler frequency constraints that the experiment imposes. Additional procedural comments will be made in the Discussion section. For now, we merely point out that vibrational structure becomes evident as one goes to lower wavelengths. Moreover, the various HSe vibrational channels depend differently on photolysis wavelength. For example, in relative terms, the $v = 0$ channel stays reasonably strong throughout the mid-UV, but the $v = 1$ channel grows in and then begins to fade as one moves to lower wavelength. Results for $v = 0$, 1, 2, and 3 at a variety of photolysis wavelengths are presented in Figure 8. Note that such behavior is not surprising given the earlier theoretical work by Schinke and co-workers for other triatomic systems.[26,27]

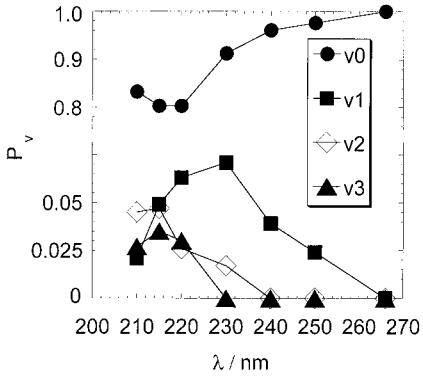

Figure 8. Branching fractions for photoprodutcs scattered into various HSe ($\Omega = {}^3/_2$) vibrational quantum states as a function of photolysis wavelength. Note that the contributions are normalized to unity.

IV. Discussion

This section is composed of two parts. In the first part, the experimental method itself is discussed. However, a complete treatment including a simulation of the experimental conditions regarding photolysis/probe alignment, beam apertures, and photolysis/probe delay is deferred to another paper.[39] In the second part of this section, the results on the photolysis of the H_2Se system are discussed.

A. Method. Experimentally, the TOF spectra shown in Figures 2 and 3 resulting from 266 nm photolysis were taken in the H-configuration. Although simply a direct TOF approach, the resolution (ΔE/E) shown here is ~0.7%. While not quite as good as the Rydberg TOF method, the resolution of the H-configuration is within a factor of 3 of that observed for typical Rydberg TOF measurements. By adjusting the apertures depicted in Figure 1, the kinetic energy resolution in Figures 2 and 3 can be improved at a cost in signal-to-noise. Note, however, that the TOF spectrum in the H-configuration has a Doppler-effect bias. All four Lyman-α transitions, $^2S_{1/2}$ (F=0,1) → $^2P_{3/2}$ and $^2S_{1/2}$ (F=0,1) → $^2P_{1/2}$, contribute to the signal, but they do not contribute evenly. There are delay-dependent biases that must to be addressed in this configuration, but a detailed discussion is deferred to another paper.[39]

A more difficult problem is encountered experimentally in this particular photolysis/probe geometry, and it becomes acute when weaker photolysis sources are used. Specifically, the H-configuration probes at zero Doppler shift, and a small background signal produced by the probe itself can become a problem when one is looking at weak signals. An advantage associated with moving to the T-configuration is the actual Doppler shift, since in practice the VADS method interrogates species moving with nonzero Doppler components. Essentially, the VADS method shifts the probe laser off the resonance frequency of probe-induced background H atoms. In the T-configuration, virtually any H atom generated by the probe is simply nonresonant and therefore not detected. In contrast, H atoms produced by the photolysis laser have significant speeds and consequently significant Doppler shifts that the T-configuration utilizes for detection.

There are two primary ways to conduct experiments in the T-configuration. One can fix the photolysis/probe delay and scan the frequency of the probe. These spectra are shown in Figure 5 for a series of delays. Here, the nuclear hyperfine F states of the H atom are monitored. Moreover, these populations can be correlated with counterfragment quantum states, since the "packet" of H atoms being probed is defined by the photolysis/

probe time delay and corresponds to a restricted set of counterfragment internal states by simple conservation of energy. The second way of conducting experiments in the T-configuration demands that one synchronously scan the photolysis/probe delay time *and* the probe laser frequency. Experimentally, one specific transition is probed. In the case of Figures 6 and 7, it was the $^2S_{1/2} \rightarrow {}^2P_{3/2}$ transition in Lyman-α out of the F = 1 nuclear hyperfine state. One can then conduct a TOF/VADS experiment. As the photolysis/probe delay is changed, H atoms travelling with a variety of speeds arrive at the detection region at a variety of times. Since the different speeds possess different Doppler shifts, the probe frquency must be scanned to maintain the resonance with the transition being monitored, in this case a specific component of the Lyman-α transition. In essence, each spectrum in Figures 6 and 7 results in a correlated state distribution. Alternatively, we could monitor the $^2S_{1/2} \rightarrow {}^2P_{3/2}$ transition in Lyman-α out of the F = 0 state instead of the F = 1 state. While in this region those two would look similar, it need not necessarily be so. In principle, it seems likely that a variety of systems can be studied with this method, i.e., it does not appear to be restricted to atomic hydrogen or H_2Se.

Finally, the use of a tunable photolysis source enables us to conduct TOF/VADS experiments as a function of photolysis wavelength. While Figures 6 and 7 show the data for four photolysis wavelengths, other wavelengths were studied and the results compiled in Figure 8. Experimentally, changing the photolysis wavelength causes an offset in the arrival time. However, the known change in photolysis energy translates directly to a change in the arrival time for a specific group of H atoms, so a TOF/VADS spectrum can be taken straightforwardly after a simple adjustment.

B. H_2Se Photolysis. Data on the ultraviolet absorption spectrum of H_2Se was reported in early work by Price et al.[40] Regarding photolysis, irradiating H_2Se in the ultraviolet is complicated, especially when secondary HSe photolysis channels are included. To a first approximation, many observable electronic exit channels exist for the photolysis of H_2Se, not including the nuclear hyperfine states in the hydrogen photofragment.[41−43] For single-photon absorption, the parent molecule can dissociate into an H atom and one of two spin−orbit states of the HSe radical

$$H{-}HSe\ (X\ ^1A_1) + h\nu \rightarrow H\ (^2S_{1/2};F) + HSe\ (X\ ^2\Pi_{3/2};v,J) \quad (1a)$$

$$H{-}HSe\ (X\ ^1A_1) + h\nu \rightarrow H\ (^2S_{1/2};F) + HSe^*\ (A\ ^2\Pi_{1/2};\ v,\ J) \quad (1b)$$

where the spin−orbit energy difference between the HSe and HSe* electronic states is 1764.2 cm^{-1}.[41] Secondary photolysis can result in six additional fragmentation pathways

$$H{-}Se\ (X\ ^2\Pi_{3/2};v,J) + h\nu \rightarrow H\ (^2S_{1/2};F) + Se\ (^3P_{J=0,1,2}) \quad (2a)$$

$$H{-}Se^*\ (A\ ^2\Pi_{1/2};v,J) + h\nu \rightarrow H\ (^2S_{1/2};F) + Se\ (^3P_{J=0,1,2}) \quad (2b)$$

making a total of eight channels. Since the energetics of the system are known, the positions of the individual pathways are readily identified. The HSe−H and H−Se bond energies are reported as D_0 = 78.99 kcal/mol and D_0 = 74.27 kcal/mol, respectively.[41] The HSe vibrational frequency is given as ω_e = 2400 cm^{-1},[44] while the rotational constant B_0 is reported to be 7.862 cm^{-1} for HSe.[41] As noted, some of the one and two photon routes result in coincidental H atom positions in the TOF spectra. A more thorough analysis of issues such as branching ratios for the various channels, however, involves polarization studies as a function of photolysis wavelength for both the primary and the secondary pathways. Here, we simply discuss the energy distributions shown in Figures 4 and 8.

The rotational data shown in Figures 3 and 4 for H_2Se photolysis are qualitatively similar to that observed for H_2S photolysis.[33] The distributions are relatively cold with intensities peaking around the first few states and falling off rather quickly. As with previous studies on HBr, the H atom nuclear hyperfine populations shown in Figure 5 are essentially statistical. Note, however, that one can conduct a VADS/TOF experiment producing results similar to Figure 5, but instead of monitoring an H_2Se photolysis channel, one can lock on to a signal derived from an HSe photolysis channel. Perhaps, the photolysis of this radical species may influence the nuclear hyperfine state populations of the H atom, but these experiments have yet to be performed.

Figure 8 presents our first insight into the underlying dynamical features associated with scattering into various HSe vibrational states as a function of H_2Se absorption wavelength. At 266 nm, virtually all of the scattering probability can be found in v = 0, even though the first four levels are energetically allowed. One can definitely see the v = 1 feature increase and then decrease again as one moves to lower wavelengths. At ∼215−220 nm, a clear competition is underway among the various vibrational states. In fact, v = 4, 5, and 6 also have measurable intensities in this region, while v = 1 is clearly on the wane. In keeping with the earlier theorerical work of Schinke and co-workers,[26,27] it is apparent that triatomic systems of this type have vibrational state populations with intriguing wavelength dependences. We present Figure 8, in part, as a coarse computational target. We also note that more detailed photolysis studies are required to explore any finer features of the various scattering resonances. Such work is ongoing in our laboratory.

Acknowledgment. We thank the Louisiana Board of Regents, the Department of Energy, the National Science Foundation, and the Center for Photoinduced Processes at Tulane University for support of this work.

References and Notes

(1) El-Sayed, M. A., Ed. *J. Phys. Chem.* **1996**, *100*, 12694−13322 (Centennial Special Issue). In particular, Butler, L. J.; Neumark, D. M. *J. Phys. Chem.* **1996**, *100*, 12801 and references therein.

(2) Schnieder, L.; Meier, W.; Welge, K. H.; Ashfold, M. N. R.; Western, C. M. *J. Chem. Phys.* **1990**, *92*, 7027.

(3) Kash, P. W.; Waschewsky, G. E.; Butler, L. J.; Francl, M. M. *J. Chem. Phys.* **1994**, *100*, 3463.

(4) (a) Cody, R. J.; Sabety-Dzvonik, M. J.; Jackson, W. M. *J. Chem. Phys.* **1977**, *66*, 2145. (b) Halpern, J. B.; Jackson, W. M. *J. Phys. Chem.* **1982**, *86*, 973.

(5) Hawkins, W. G.; Houston, P. L. *J. Chem. Phys.* **1980**, *73*, 297.

(6) Vasudev, R.; Zare, R. N.; Dixon, R. N. *J. Chem. Phys.* **1984**, *80*, 4863.

(7) Qian, C. X. W.; Noble, M.; Nadler, I.; Reisler, H.; Wittig, C. *J. Chem. Phys.* **1985**, *83*, 5573.

(8) Radhakrishnan, G.; Ng, D.; Estler, R. C. *Chem. Phys. Lett.* **1981**, *84*, 260.

(9) Hradil, V. P.; Suzuki, T.; Hewitt, S. A.; Houston, P. L.; Whitaker, B. J. *J. Chem. Phys.* **1993**, *99*, 4455.

(10) (a) Chandler, D. W.; Thoman,J. W., Jr.; Janssen, M. H. M.; Parker, D. H. *Chem. Phys. Lett.* **1989**, *156*, 151. (b) Chandler, D. W.; Janssen, M. H. M.; Stolte, S.; Strickland, R. N.; Thoman, Jr., J. W.; Parker, D. H. *J. Phys. Chem.* **1990**, *94*, 4839.

(11) Woodbridge, E. L.; Fletcher, T. R.; Leone, S. R. *J. Chem. Phys.* **1988**, *92*, 5387.
(12) Houston, P. L. *J. Phys. Chem.* **1987**, *91*, 5388.
(13) (a) Xu, Z.; Koplitz, B.; Buelow, S.; Baugh, D.; Wittig, C. *Chem. Phys. Lett.* **1986**, *127*, 534. (b) Xu, Z.; Koplitz, B.; Wittig, C. *J. Chem. Phys.* **1987**, *87*, 1062. (c) Xu, Z.; Koplitz, B.; Wittig, C. *J. Phys. Chem.* **1988**, *92*, 5518. (d) Xu, Z.; Koplitz, B.; Wittig, C. *J. Chem. Phys.* **1989**, *90*, 2692.
(14) Mo, Y.; Tonokura, K.; Kawasaki, M.; Sato, T.; Arikawa, T.; Reilly, P. T. A.; Xie, Y.; Yang, Y.; Huang, Y.; Gordon, R. J. *J. Chem. Phys.* **1992**, *97*, 4815.
(15) Gericke, K.-H.; Klee, S.; Comes, F. J.; Dixon, R. N. *J. Chem. Phys.* **1986**, *85*, 4463.
(16) Docker, M. P.; Ticktin, A.; Bruhlamann, U.; Huber, J. R. *J. Chem. Soc., Faraday Trans*. 2 **1989**, *85*, 4463.
(17) Zhang, Q.; Kandel, S. A.; Wasserman, T. A. W.; Vaccaro, P. H. *J. Chem. Phys.* **1992**, *96*, 1640.
(18) Buntine, M. A.; Chandler, D. W.; Hayden, C. *J. Chem. Phys.* **1992**, *97*, 707.
(19) Imre, D.; Kinsey, J. L.; Sinha, A.; Krenos, J. *J. Chem. Phys*. **1984**, *88*, 3956.
(20) Green, W. H., Jr.; Moore, C. B.; Polik, W. F. *Annu. Rev. Phys. Chem.* **1992**, *43*, 591 and references therein.
(21) Moore, D. S.; Bomse, D. S.; Valentini, J. J. *J. Chem. Phys.* **1983**, *79*, 1745.
(22) Chandler, D. W.; Houston, P. L. *J. Chem. Phys.* **1987**, *87*, 1445.
(23) Reid, S. M.; Reisler, H. J.; *J. Chem. Phys*. **1994**, *101*, 5683.
(24) Shafer, N.; Satyapal, S.; Bersohn, R. *J. Chem. Phys.* **1989**, *90*, 6807.
(25) Crim, F. F. *Annu. Rev. Phys. Chem.* **1984**, *35*, 657.
(26) (a) Schinke, R.; Engel, V. *Chem. Phys. Lett.* **1986**, *124*, 504. (b) Engel, V.; Schinke, R.; Staemmler, V. *Chem. Phys. Lett.* **1986**, *130*, 413.
(27) Schinke, R.; Engel, V. *J. Chem. Phys.* **1990**, *93*, 3253.
(28) Zacharias, H.; Rottke, H.; Danon, J.; Welge, K. H. *Opt. Commun.* **1981**, *37*, 15.
(29) Krautwald, H. J.; Schneider, L.; Welge, K. H.; Ashfold, M. N. R. *Faraday Discuss. Chem. Soc*. **1986**, *82*, 99.
(30) Dixon, R. N.; Nightingale, J.; Western, C. M.; Yang, X. *Chem. Phys. Lett*. **1988**, *151*, 328.
(31) Cromwell, E. F.; Stolow, A.; Vrakking, M. J. J.; Lee, Y. T. *J. Chem. Phys.* **1992**, *97*, 4029.
(32) Segall, J.; Wen, Y.; Singer, R.; Dulligan, M.; Wittig, C. *J. Chem. Phys.* **1993**, *99*, 6600.
(33) Wilson, S. H. S.; Howe, J. D.; Ashfold, M. N. R. *Mol. Phys.* **1996**, *88*, 841.
(34) Xu, K.; Zhang, J. *J. Chem. Phys.* **1999**, *111*, 3783.
(35) Schneider, L.; Seekamp-Rahn, K.; Wrede, E.; Welge, K. H. *J. Chem. Phys.* **1997**, *107*, 6175.
(36) Cowen, K. A.; Lorenz, K. T.; Yen, Y.-F.; Herman, M. F.; Koplitz, B. *J. Chem. Phys.* **1995**, *103*, 5864.
(37) Lorenz, K. T.; Cowen, K. A.; Fleming, P. F.; Mathews, M. G.; Herman, M. F.; Koplitz, B. *Chem. Phys. Lett.* **1996**, *261*, 145.
(38) Hollas, J. M. *Modern Spectroscopy*; Wiley: New York, 1987.
(39) Zhang, X.; Johnson, M.; Lorenz, K. T.; Koplitz, B. Unpublished results.
(40) Price, W. C.; Teegan, J. P.; Walsh, A. D. *Proc. R. Soc. A* **1950**, *201*, 600.
(41) Gibson, S. T.; Greene, J. P.; Berkowitz, J. *J. Chem. Phys.* **1986**, *85*, 4815.
(42) Lindgren, B. *J. Mol. Spectrosc.* **1968**, *28*, 536.
(43) Dobson, D. C.; James, F. C.; Safarik, I.; Gunning, H. E.; Strausz, O. P. *J. Chem. Phys.* **1975**, *79*, 771.
(44) Huber, K. P.; Herzberg, G. *Molecular Spectra and Molecular Structure IV. Constants of Diatomic Molecules*; Van Nostrand Reinhold: New York, 1979.